



Serum-based Raman spectroscopic diagnosis of blast-induced brain injury in a rat model

MEILAN GE,^{1,2} YUYE WANG,^{1,2,*} TONG WU,³ HAIBIN LI,^{1,2}
CHUANYAN YANG,⁴ TUNAN CHEN,⁴ HUA FENG,⁴ DEGANG XU,^{1,2}
AND JIANQUAN YAO^{1,2}

¹*School of Precision Instruments and Optoelectronics Engineering, Tianjin University, Tianjin 300072, China*

²*Key Laboratory of Optoelectronics Information Technology (Ministry of Education), Tianjin University, Tianjin 300072, China*

³*School of Marine Science and Technology, Tianjin University, Tianjin 300072, China*

⁴*Department of Neurosurgery and Key Laboratory of Neurotrauma, Southwest Hospital, Third Military Medical University (Army Medical University), Chongqing 400038, China*

*yuyewang@tju.edu.cn

Abstract: The diagnosis of blast-induced traumatic brain injury (bTBI) is of paramount importance for early care and clinical therapy. Therefore, the rapid diagnosis of bTBI is vital to the treatment and prognosis in clinic. In this paper, we reported a new strategy for label-free bTBI diagnosis through serum-based Raman spectroscopy. The Raman spectral characteristics of serum in rat were investigated at 3 h, 24 h, 48 h and 72 h after mild and moderate bTBIs. It has been demonstrated that both the position and intensity of Raman characteristic peaks exhibited apparent differences in the range of 800-3000cm⁻¹ compared with control group. It could be inferred that the content, structure and interaction of biomolecules in the serum were changed after blast exposure, which might help to understand the neurological syndromes caused by bTBI. Furthermore, the control group, mild and moderate bTBIs at different times (a total of 9 groups) were automatically classified by combining principal component analysis and four machine learning algorithms (quadratic discriminant analysis, support vector machine, *k*-nearest neighbor, neural network). The highest classification accuracy, sensitivity and precision were up to 95.4%, 95.9% and 95.7%. It is suggested that this method has great potential for high-sensitive, rapid, and label-free diagnosis of bTBI.

© 2023 Optica Publishing Group under the terms of the [Optica Open Access Publishing Agreement](#)

1. Introduction

Blast-induced traumatic brain injury (bTBI) refers to a traumatic brain disorder caused by a shock wave, which results in the head suddenly accelerate or decelerate [1]. Defense and Veterans Brain Injury Center (DVIBIC) reported that about 413,858 personnel had been diagnosed with bTBI between the years of 2000 and 2019 in U.S. army [2]. In addition, bTBI also is an increasing problem in civilian practice caused by industrial accidents [3–5], which leads to a major health and economic burden [6]. It is demonstrated that most of the patients with bTBI develop some symptoms, e.g. cognitive dysfunction, memory loss, attention difficulties, and impaired balance [7–9]. Importantly, many of these symptoms may not be immediately apparent and may only manifest months to years after the initial injury, which seriously affect the physical and mental well-being of the patients [10]. Furthermore, it has been shown that mild bTBI is often omitted by clinicians due to the lack of visible symptoms and high-sensitivity diagnosis method, compared with detectable severe trauma [11]. Therefore, it is urgent to develop a rapid and high-sensitivity diagnostic method for bTBI, especially for mild bTBI.

Currently, the existing diagnosis methods for bTBI mainly include neurobehavioral evaluations, neuroimaging, and biomarker methods according to the different detection principles. As for

typical neurobehavioral evaluation technologies, the Glasgow Coma Scale (GCS) and the Military Acute Concussion Evaluation (MACE) can be used to initially determine the severity of bTBI. However, MACE should be used by trained medics and corpsmen as close to the time of injury as possible [12]. And GCS may result in errors in many cases due to relying on subjective approach [13]. Computed tomography (CT) and magnetic resonance imaging (MRI) are routinely performed to evaluate injuries in clinic neuroimaging. However, patients with mild bTBI often have normal brain CT and MRI [14]. Moreover, biomarker method as a new technology has drawn wide attention. Several biomarkers have been reported as diagnostic markers for bTBI, and the content changes are related to the time after trauma [8,15,16]. However, the measurement methods of biomarkers are time-consuming and expensive, such as high-performance chromatography (HPLC) and enzyme-linked immunosorbent assay (ELISA) [15]. Thus, a rapid, high-sensitive, economical, label-free diagnosis tool is urgently wanted for bTBI.

Serum is the most widely used biofluid for non-invasive disease assessment because of minimal invasiveness and convenient collection in clinical practice. It contains many biological molecules, i.e. lipids, proteins, carbohydrates, nucleic acids [17]. To date, most of the potential biomarkers have been identified in serum. It has been demonstrated that the changes of some biomarkers in the serum levels have been found at different time points with different severities of bTBI, such as the glial protein S100 β , neurofilament heavy chain (NF-H), neuron-specific enolase (NSE), myelin basic protein (MBP), ubiquitin carboxy-terminal hydrolase-L1 (UCH-L1) [8,15,16]. Thus, monitoring serum at various time points after bTBI can help identify the pathological processes in bTBI. Raman spectroscopy is the inelastic interaction between laser light and molecules, which has been widely applied in analyzing and identifying vibration and/or rotation information of various compounds due to its fingerprint characteristic. It has gained interest in biomedical fields as a label-free, high resolution and non-invasive monitoring modality, which is capable of detecting structure changes and biochemistry of molecular in real time [18,19]. Particularly, Raman spectroscopy technology is negligible interference from water potential and therefore is appropriate for the biofluid sample. Thus, it is an ideal method for diagnosis bTBI via monitoring the temporal Raman characteristic changes of serum.

In this paper, we proposed a new strategy for the diagnosis of bTBI using the serum-based Raman spectroscopy. The Raman spectra of serum after mild and moderate bTBIs were investigated at 3 h, 24 h, 48 h, 72 h in 800-3000 cm^{-1} region. Compared with the control group, the locations and intensities of Raman characteristic peak showed clear differences at different time points after mild and moderate degrees of bTBI. This main reason was that the structure, content and interaction of biomolecules in serum was one the key reasons for symptom of bTBI. Moreover, the principal component analysis and machine learning algorithms were used together in Raman spectra of serum to automatically identify the different times after different severity of bTBI. The highest diagnostic accuracy was up to 95.4%. The results of this study provided a high-sensitivity, rapid and minimally invasive method for early diagnosis of bTBI.

2. Samples and methods

2.1. Sample preparation

2.1.1. bTBI models

A reproducible measurement protocol was established by standardizing all experimental steps of sample preparations. The adult male Sprague-Dawley rats weighing about 250 g were adopted to establish the bTBI model. All the rats were purchased from the Third Military Medical University (Chongqing). All animal experiments were performed by the China Animal Welfare Legislation and were approved by the Third Military Medical University Committee on Ethics for the Care and Use of Laboratory Animals. The shock wave was generated by a compressed air-driven bio-shock tube (Daping Hospital of the Third Military Medical University). Unanesthetized rats

were fixed into individual cages in order to prevent the subsequent injuries. A pressure gauge was used to measure the pressure of shock waves. The pressure peaks of gauge were set to 4 MPa and 5 MPa, which corresponded to the mild and moderate groups. The established model was validated using modified neurological severity score (mNSS), and the results were consistent with the our previous work [20]. The rats were randomly divided into three groups: control group (without shock wave exposure), mild and moderate, where the numbers of corresponding groups were 5, 20 and 20, respectively.

2.1.2. Serum collection

Figure 1(a) depicted the schematic diagram of the sample preparation. Plasma samples were collected from the hearts of anesthetized rats by using heart exsanguination at 3 h, 24 h, 48 h, 72 h after mild and moderate blast exposure. The control group samples were collected by the same way. Here, the number of plasma samples at each time point after different bTBI was 5 for reproducibility assessment. The extracted plasma samples stood for one hour at room temperature. Then the plasma was centrifuged with 4500 r/min for 10 min to obtain the separated serum sample. All samples were stored at -80°C until experimental measurement. The samples were thawed at room temperature about 20 min before Raman experiment. A drop (about $50\mu\text{L}$) of each serum sample was transferred to a glass slide with groove.

2.2. Raman spectroscopic experimental setup

The Raman spectra of serum samples were measured by using Raman microscope system (Ondax, SureBlockTM Inc. Monrovia, CA, USA), as shown in Fig. 1(b). The excitation laser (785 nm) was focused on the sample by a 10X objective lens. The collected signal was filtered through filters to remove the Rayleigh scattering light. The filtered signal was focused into spectrometer (Horiba, iHR320, Japan) within a 1200 grooves/mm grating via a fiber, and was detected by a CCD detector (Syncerity, Horiba, Japan). The initial spectra of serum samples were $0\text{--}3000\text{cm}^{-1}$ region with a resolution of 2.5cm^{-1} . The analysis range of Raman spectrum was chosen as $800\text{--}3000\text{cm}^{-1}$ due to the most of characteristic peaks concentrating in this range. The final Raman spectrum of each sample was the averaged result of the spectra at multiple different positions, in which the spot does not overlap for each measurement. At each position, a spectrum was recorded using a laser power of 190 mW and a 10s acquisition time. The experimental temperature was maintained at $25 \pm 2^{\circ}\text{C}$ during the whole experiment. Accordingly, the final Raman spectrum of each group was the average result of the five samples with multiple measurement at different positions.

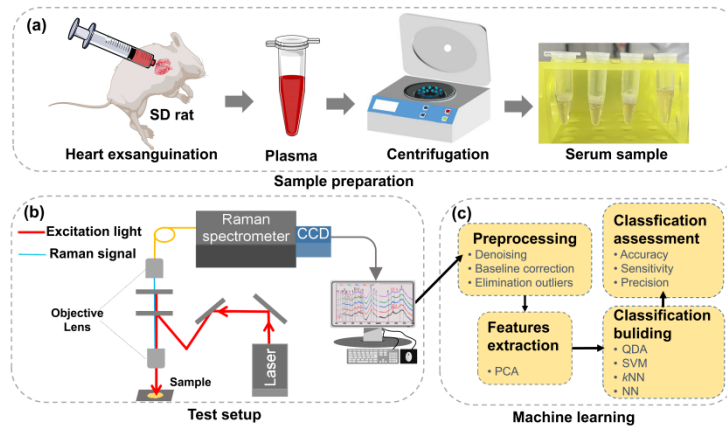


Fig. 1. The schematic diagram of (a) sample preparation, (b) Raman experimental setup, (c) classification system.

2.3. Spectral analysis

On account of the fluctuations of measurement system and environment, there were deviations in recorded spectral data. Therefore, it is necessary to adopt effective preprocessing method for the raw Raman spectral data, as shown in Fig. 1(c). The data preprocessing method was divided into three stages: denoising, baseline correction, elimination outliers. Firstly, the Savitzky-Golay smoothing method (3rd polynomial order, 79 smoothing points) was applied to denoising. Secondly, the baseline of spectrum was corrected to eliminate the fluorescence background of serum sample by using 5 order polynomials. Finally, the interquartile method was used to remove the outliers. An example of the Raman spectrum of the control group was given to explain the preprocessing process in details. Fig. S1(a) showed the raw Raman spectrum of serum from control group. Fig. S1(b) and (c) exhibited the Raman spectra after denoising and baseline correction in turn. Fig. S1(d) showed the elimination outliers of the Raman spectra of the control group. It can be seen that the spectral features can be well kept before and after preprocessing. The spectral numbers after preprocessing data were listed in Table 1.

Table 1. Raman spectra number of serum sample.

Sample group	3h	24h	48h	72h	Total
Mild bTBI	39	102	65	93	299
Moderate bTBI	33	61	76	68	238
Control group					65

Generally, there was redundant information in Raman spectra of bTBI. The all preprocessed data was subjected to principal component analysis (PCA) to extract the features and reduce the dimension of Raman spectra. PCA is performed on the original data in order to define a new dimensional space by using a small number of components. In PCA, the original data are transformed into uncorrelated components that explain the most variance in the original data, in which transformed components are called as principal components (PCs). PCA is concerned with data reduction and commonly used as a preliminary step of high-dimensional data analysis, followed by further multivariate statistical methods [21]. Considering the imbalance of data set used in classification, four machine learning classifier algorithms, including quadratic discriminant analysis (QDA), support vector machine (SVM), k -near neighbor (k -NN) and neural network (NN), were applied to classify and identify control group, mild and moderate bTBIs after 3 h, 24 h, 48 h, 72 h ($n = 9$ group). The QDA is a kind of discriminant analysis method, which generalized the linear discriminant analysis classifier to the case of distinct covariance matrices among classes. For the QDA classifier, an accurate estimation of the covariance matrices is required to yield high classification performance. The QDA algorithm is more flexible because it can learn nonlinear boundaries between classes. It is suitable for situations with multi-category classification, and without parameter tuning [22,23]. Support vector machine (SVM) is a utilized supervised learning algorithm [24], which has a good performance on higher dimensional data. Given data points distributed on the feature space, SVM aims to find a hyperplane that separates all data points of one class from those of another class, which maximizes the distance between the classes. For SVM algorithm, the selection of the kernel function and error penalty is the key factor of influencing the performance of model [25]. In addition, SVM-based classifiers work well in dealing with a small data set, and they have a good generalization ability [26]. k NN is one of practical algorithms. The basic idea is that an object can be represented by a majority vote of its neighbors, with the object being assigned to the category among its k nearest neighbors. The definition of the distance is directly related to the selection of the k nearest neighbors and affects its classification accuracy. The k NN-based classifier is relatively simple and easy to use. They are suitable to solve multi-category classification, and insensitive to outliers [27,28]. Neural network (NN) is sample optimization algorithm modeled on the neuronal signal processing

characteristics of the brain. It mimics the behavioral characteristics of animal neural networks for distributed parallel information processing. It is well known that there are different types of NN according to their structure and learning process. In this work, we chosen the feedforward NN, in which all connections between neurons were set up in one direction from network's input towards the output. The network architecture was consistent with the Refs. [29], which included an input layer, a hidden layer, and an output layer. Epoch and learning rate are an important hyperparameters for NN algorithm, which have a great influence on the accuracy and time of model training. Generally, the epoch and learning rate value with the highest training accuracy are selected to the final parameter for the model training. The NN-based classifier has strong robustness and fault tolerance due to its ability to adequately approximate complex nonlinear relationship [30].

Before classification, all data of Raman spectra of control group and bTBI groups at different times ($n = 9$ group) after PCA was randomly divided into 80% as training set, and 20% as test set. The data of training set was the input data to the QDA, SVM, k NN and NN classifiers, respectively. In order to establish a stable and reliable training model, the 5-fold cross validation was utilized in classifier training to prevent the overfitting and underfitting. Namely, the training data are divided into five subsets of equal size, where four subsets are used to train the models and the remaining one is reserved for the purpose of validation and calculating error. That means there are five times training and validation with different subsets. The final training result of each model is the average of the results of five times [31]. Then the trained QDA, SVM, KNN classifiers were performed to predict the test set. In order to ensure the reliability of the classification and prediction results, the data of each group was randomly divided into training set and test set three times. The training and prediction of each classifier were performed based on the data set of these three times, respectively. It should be mentioned that the related parameters of training model were kept the same for the three times. The final result was the average of the results of three times prediction. The parameters of accuracy, sensitivity and precision were used to evaluate the performance of each classifier according to the confusion matrix.

3. Results and discussion

3.1. Raman spectroscopy

Figure 2 showed the Raman spectra of serum in rats at 3 h, 24 h, 48 h, 72 h time points after mild bTBIs in $800\text{--}3000\text{cm}^{-1}$ region compared with the control group, where the positions of all characteristic peaks were labeled. The assignments of all Raman spectra were summarized in Table S1 of supplementary according to the previous works [32–36]. Overall, the position of nineteen Raman characteristic peaks at 3 h, 24 h, 48 h, 72 h after mild bTBI were basically consistent with the control group, which were the peaks at 811, 852, 940, 966, 1003, 1030, 1058, 1126, 1172, 1205, 1247, 1270, 1344, 1400, 1415, 1447, 1658, 1723, 1778, 2854, 2882 and 2932cm^{-1} (marked in black color), respectively. However, some positions marked in red color of Raman characteristic peaks were not exact the same at 3 h, 24 h, 48 h, 72 h after mild bTBI compared with control group. Table 2 showed the summary of the changed positions of Raman characteristic peaks after mild bTBI. It was seen that the characteristic peaks at 804, 913, 1304cm^{-1} in control group shifted to 811, 902, 1314cm^{-1} at 3 h, 24 h, 48 h, 72 h after mild blast exposure, respectively. It could be attributed to that the concentration of collagen, lipids, nucleic acid in serum has changed at 3 h, 24 h, 48 h, 72 h after mild bTBI. Meanwhile, the interaction among them might result in the conformation changes. Furthermore, the position peak at 1146cm^{-1} in control group was changed to 1156cm^{-1} both at 3 h, 24 h and 72 h, whereas it shifted to 1149cm^{-1} at 48 h. The shifts of these peaks could verify that the interaction among biological molecules in serum were changed after mild bTBI. Moreover, the Raman peaks at 1103cm^{-1} were shown at 3 h, 24 h, 48 h and control group, but disappeared at 72 h after bTBI. It could be attributed that the level of amide I was reduced to the point which cannot be measured

at 72 h after blast exposure. The Raman peaks at 877cm^{-1} only existed in control group. It indicated the vibration of choline or phospholipids became so weak after bTBI, which could not be detected. Additionally, the Raman peak at 1077cm^{-1} showed up at 3 h, 24 h, 48 h after mild bTBI, but it disappeared for control group and mild bTBI at 72 h. It might be due to that the content of lipids associated with the peak at 1077cm^{-1} changed over time after mild bTBI.

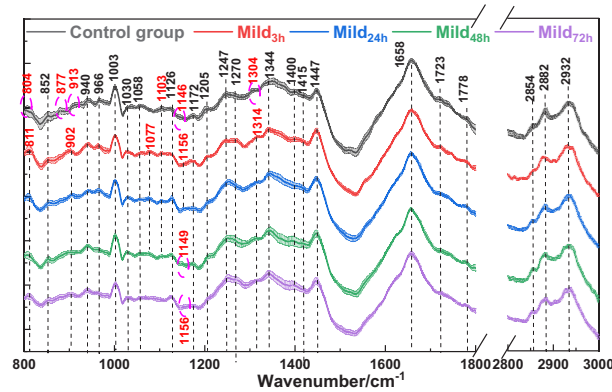


Fig. 2. The Raman spectra of mild bTBI at different time points.

Table 2. The Raman peak positions at different time points after mild bTBI.

Sample group	Control	Mild _{3h}	Mild _{24h}	Mild _{48h}	Mild _{72h}
The Raman peak position/ cm^{-1}	804	811	811	811	811
	877				
	913	902	902	902	902
		1077	1077	1077	
	1103	1103	1103	1103	
	1146	1156	1156	1149	1156
	1304	1314	1314	1314	1314

Then, the serum Raman spectra of moderate bTBI at different time points were shown in Fig. 3, where the positions of all characteristic peaks were labeled. The assignments of the Raman peaks were summarized in Table S1 of supplementary. On the whole, the positions of 23 Raman characteristic peaks at 3 h, 24 h, 48 h, 72 h after moderate bTBI basically coincided with control group, where the peaks were $855, 877, 940, 964, 1003, 1030, 1059, 1102, 1126, 1172, 1205, 1247, 1272, 1344, 1397, 1415, 1447, 1657, 1723, 1778, 2854, 2882, 2934\text{cm}^{-1}$ (marked in black color). But some Raman characteristic peak positions after moderate bTBI marked in red color in Fig. 3 were changed, which has been summarized in Table 3. The Raman peaks at 804 and 913cm^{-1} in control group were shifted to 810 and 905cm^{-1} after moderate bTBI. The Raman peak at 1146cm^{-1} in control group was shifted to $1154, 1152, 1152, 1154\text{cm}^{-1}$ at 3 h, 24 h, 48 h, 72 h, respectively. There might be two reasons. On one hand, the shift of Raman peaks can be attributed to that the interactions among biomolecules, such as carotenoids glycogen and protein changed with time increasing. On the other hand, these shifts might be caused by the conformational changes of biomolecules in serum [37]. Furthermore, the characteristic peak at 1304cm^{-1} in control group was shifted to 1312cm^{-1} after bTBI at 3 h, 24 h, 48 h, but it disappeared at 72 h after bTBI. The reason for this phenomenon was that the interaction among amid III, fatty acid chains in rat serum was changed at 3 h, 24 h and 48 h after moderate bTBI.

compared with the control group. And the concentration of these biological molecules was too low to be detected after moderate bTBI at 72 h. The Raman peak at 1074cm^{-1} showed up only at 3 h, 24 h and 48 h after bTBI. Overall, considering these Raman characteristic peaks were assigned to the vibration of proteins, lipids, collagen, glycogen, nucleic acid, phospholipids, cyclohexane, and other biomolecules, it could be concluded that the changes of characteristic peaks with time after bTBI were related to the conformation changes of these biomolecules in serum. Such changes may affect the normal function of brain, leading to the symptoms of neurological impairment.

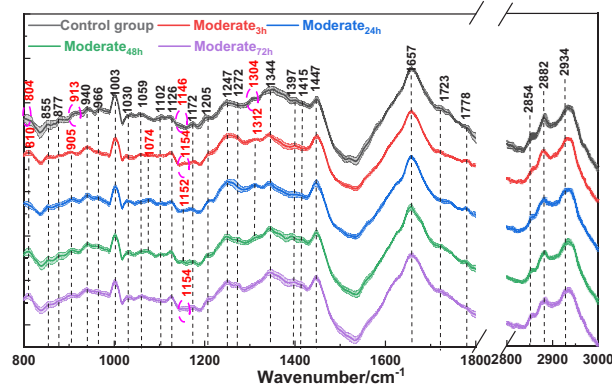


Fig. 3. The Raman spectra of moderate bTBI at different time points.

Table 3. The Raman peak positions at different time points after moderate bTBI.

Sample group	Control	Moderate _{3h}	Moderate _{24h}	Moderate _{48h}	Moderate _{72h}
The Raman peak position/ cm^{-1}	804	810	810	810	810
	913	905	905	905	905
		1074	1074	1074	
	1146	1154	1152	1152	1154
	1304	1312	1312	1312	

Furthermore, the comparisons of location changes of Raman peaks over time after mild and moderate bTBIs were shown in Fig. 4, where the 804 , 913 , 1074 , 1146 and 1304cm^{-1} were chosen to analyze. Despite the small differences of $1\text{--}3\text{ cm}^{-1}$, the trends of shifted change with 804 , 913 and 1146cm^{-1} were in complete agreement after mild and moderate bTBIs. It was obvious that the shift of Raman peaks at 804 , 913 , 1146cm^{-1} existed throughout 72 h after bTBI. For the peak at 1304cm^{-1} , the mild bTBI exhibited the same trendline of change with moderate bTBI within 72 h, except for the 72 h time point after moderate bTBI. From the Fig. 4(c), the Raman peak at 1074cm^{-1} occurred at 3 h but disappeared at 72 h, which was observed in both mild and moderate bTBIs. Overall, there were shifts of Raman peak position both mild and moderate bTBIs. These results demonstrated that, the Raman spectra of serum was sensitive for bTBI, especially for mild bTBI. For mild bTBI, the apparent differences of serum Raman spectra between mild bTBI and control group began 3 h after injury. It indicated that it was an effective and high-sensitive method for early diagnosis of mild bTBI based on Raman spectra of serum.

Moreover, the changing trends of Raman intensity in rat serum versus time after mild and moderate bTBIs were shown in Fig. 5(a) and (b) respectively, where the Raman intensity of peaks at 966 , 1003 , 1058 , 1126 , 1205 , 1247 , 1344 , 1447 , 2854cm^{-1} were chosen. For better

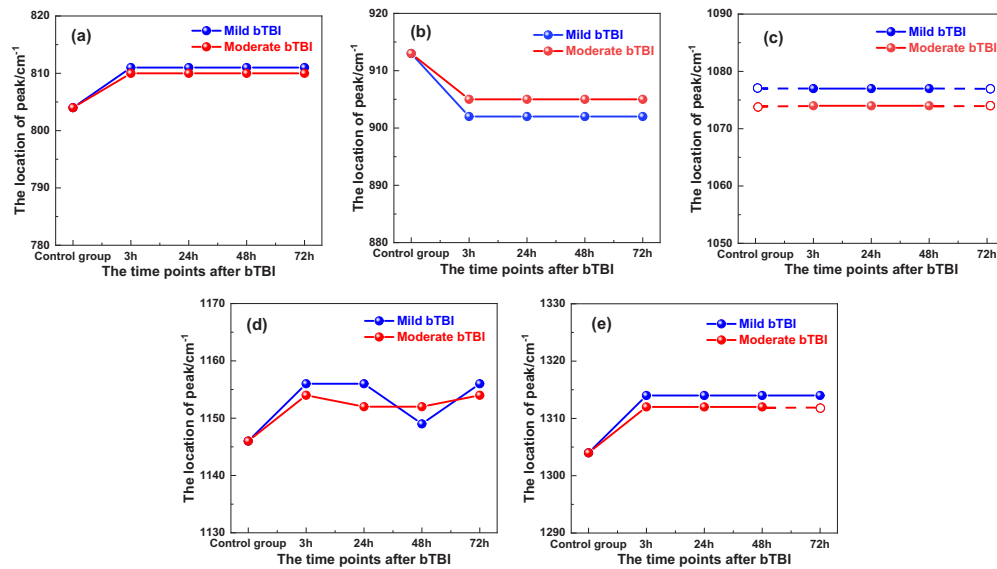


Fig. 4. The comparison of location changes of peaks at (a) 804cm^{-1} , (b) 913cm^{-1} , (c) 1074cm^{-1} , (d) 1146cm^{-1} and (e) 1304cm^{-1} over time after mild and moderate bTBIs. (The hollow circles and dotted line indicate the Raman peaks disappear at the corresponding time points.)

comparison, the Raman intensity of control group was set as that at 0 h. The Y-axis was the Normalized Raman intensity of different peaks. It could be seen the temporal changes of Raman intensities at these peaks were observed in both mild and moderate blast exposure. From Fig. 5(a), the Raman intensities of the peaks at 966 , 1126 and 1344cm^{-1} all decreased monotonously with time increasing (3 h, 24 h, 48 h, 72 h) after bTBI compared with control group. The intensity at 1003 , 1058 , 1205 , 2854cm^{-1} all showed a monotonous decrease firstly at 3 h and 24 h compared with control group. Then, with the time increasing after blast exposure, these peak intensities increased at 48 h and began to decline at 72 h, especially the peak at 1058cm^{-1} significantly increased at 48 h after bTBI. It was attributed that the content of biomolecules related to the peak arose notably increase at 48 h after mild bTBI. The Raman intensity of the peak at 1247cm^{-1} decreased and reached the minimum at 3 h, then began to increase slowly. Moreover, the Raman intensity at 1447cm^{-1} increased at 3 h after mild bTBI compared with control group, whereas a gradual decrease tendency could be observed with the time increasing. The Raman intensity exhibited recovery trend among 1058 , 1205 , 1247 and 2854cm^{-1} . However, there was no recovery trend at 72 h after mild blast exposure at 966 , 1003 , 1126 , 1344 and 1447cm^{-1} .

Comparatively, it was seen from Fig. 5(b) that, the Raman intensities of peaks at 966 , 1003 , 1058 , 1126 , 1205 , 1247 , 1344 , 1447 and 2854cm^{-1} were significant different from that of the control group. The intensity of Raman peaks at 966 , 1003 , 1058 , 1126 , and 1447cm^{-1} decreased firstly and achieved the minimum at 3 h after blast exposure, then it showed a gradual increasing trend at 24 h and 48 h. Especially, the intensity of these five peaks exhibited a recovery trend at 72 h after moderate bTBI. This was caused by the changes of lipids, proteins and phenylalanine level in serum. As for the peak at 1344cm^{-1} , its changing trend of intensity was consistent with above five peaks at 3 h, 24 h, 48 h compared with control group, but the intensity had a dramatically decreased at 72 h after moderate blast exposure. Moreover, the Raman intensity at 1205 and 1247cm^{-1} decreased firstly at 3 h and then increased at 24 h after bTBI. Then a gradual tendency to return to normal level could be observed at subsequent times (48 h and 72 h).

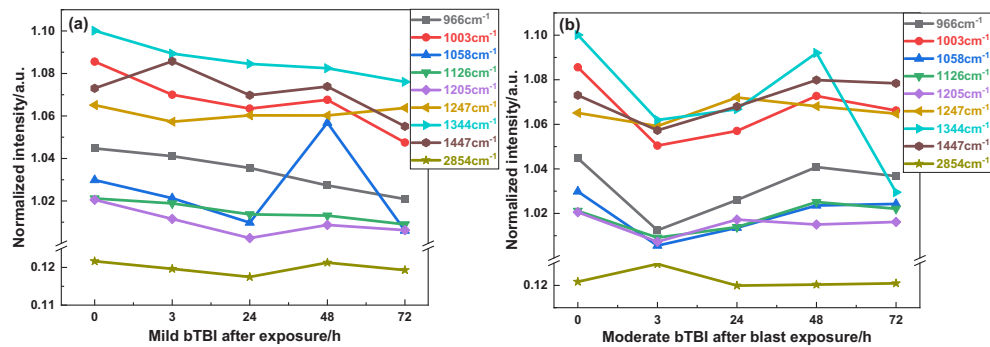


Fig. 5. The Raman intensities change of (a) mild and (b) moderate bTBI.

Additionally, the Raman intensity of peaks at 2854cm^{-1} showed an increasing trend at 3 h after moderate bTBI, then it followed a recovery trend with time increasing. Note that the changing trends of Raman characteristic intensity of moderate bTBI were not consistent with those in mild bTBI. And the Raman intensity of moderate bTBI had more significant changes. Moreover, the recovery tendency of Raman intensity during 72 h can reflect that the organism has ability to repair itself.

3.2. Classification

The Raman spectra of serum at different time points after different traumatic degrees were classified and identified using a method combining PCA and machine learning classifiers. The all preprocessed data listed in Table 1 were transformed to PCA to reduce the dimensions of process data and improve the efficiency of classification, as shown in Fig. 6. The dimension of Raman spectrum fell from 4223 to 441 after PCA processing. Figure 5(a) exhibited the cumulative contribution to the total variance of serum spectra, and the inset was the eigenvalue of each PC. And it was obvious that the eigenvalues declined sharply with the increasing PC numbers. It is seen that the first 3 PCs can describe the main characteristics of original serum data, where the cumulative percentage variance of the first 3 PCs was up to 93.8%. However, considering the other PCs also had the important feature information for classification despite they contained low cumulative variance, the choice of PCs number should be further optimized according to the classification results. In this work, the first 10 PCs were chosen as an input variable for classification, where the cumulative percentage variance was up to 97.0%. The score of serum samples on the first two PCs was shown in Fig. 6(b), in which the confidence ellipse was plotted based on 95.0% confidence interval. The PC1 and PC2 components explained 84.4% and 7.7% of the total variance in the spectra of serum samples, respectively. Each color scatter represents different group sample. As can be seen from Fig. 6(b), each group had good clustering results except only a few samples falling outside their confidence ellipses. However, the separation effect based on the PCA model of bTBI at different time points (total = 9 group) should be improved further. The reason for this is that the biological information in serum show similarity after mild and moderate bTBIs.

Based on the PCA results, the machine learning algorithms were used to classify the control group, mild and moderate bTBIs at different times to improve the identification performance. In the process of model training, 5-fold cross validation was used based on the training set. Then the trained models were performed to predict the control group, mild and moderate bTBIs at different times based on test set. The hyperparameters were selected according to the highest accuracy after 5-fold cross validation based on training set. In SVM algorithm, quadratic function was introduced as kernel function. The parameter of k was set to 3, and the Euclidean distance was

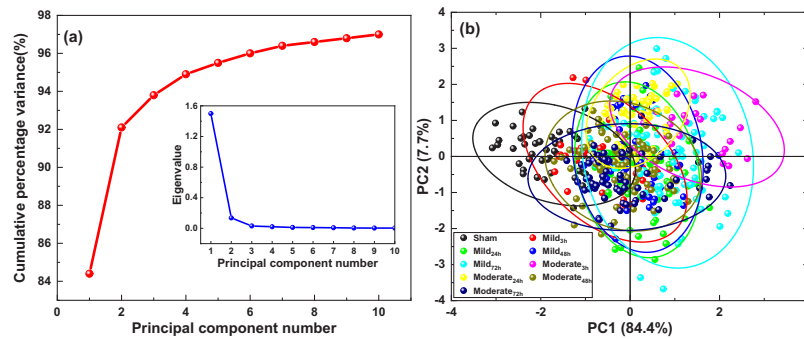


Fig. 6. Analysis results of PCA. (a) cumulative percentages of the variance of the first 10 PCs, (b) scores of serum samples on the first two PCs.

adopted in k NN classifier model. The training accuracy of SVM classifier was exhibited in Fig. S2 with the PCs number changing from 3 to 11. As can be seen from the Fig. S2, the training accuracy increased to the maximum when the PCs number increased from 3 to 10, whereas the accuracy reduced slightly with larger PCs number due to the introduction of redundant information. Thus, it was reasonable that the first 10 PCs were used as an input variable for classification, which can describe the characteristics of original serum data more accurately. NN model uses the fully connected feed-forward neural network, in which the activation function was ReLU. Additionally, the value of the number of fully connected layer and the layer size were set to 1 and 100, respectively. The epoch of NN classifier was set to 1000 according to the optimal training accuracy and training time, which has been shown in Fig. S3. The prediction quality of each classifier was shown in the confusion matrix of Fig. 7. Figure 7(a)-(d) corresponded to QDA, SVM, k NN and NN classifiers respectively, where the number represented the classification accuracy of each class based on test set. The diagonal value was the classification accuracy. And it had better classification performance for this class when the value was closer to 100%. It was seen from Fig. 7 that each classifier showed different classification result for different classes. It should be noted from Fig. 7(a) that QDA classifier had excellent classification among Mild_{72h}, Moderate_{3h}, Moderate_{24h}, Moderate_{3h} and Moderate_{3h} group. However, the Mild_{3h} and Mild_{48h} groups exhibited poor results. For SVM classifier, the accuracy of each class was greater than 90%, especially the four categories of Mild_{3h}, Mild_{72h}, Moderate_{3h} and Moderate_{72h} were up to 100%. It had prominent results for Mild_{24h}, Mild_{72h}, Moderate_{3h} and Moderate_{48h} classes based on k NN classifier, as shown in Fig. 7(c). Additionally, the control, Mild_{3h}, Mild_{72h}, Moderate_{3h} and Moderate_{48h} groups all exhibited remarkable classification results based on the NN classifier. But the Mild_{48h} had an unsatisfactory prediction, which was easy to be misclassified to Mild_{24h}, Moderate_{48h} and Moderate_{72h}, as shown in Fig. 7(d). Furthermore, it was worth noting that, both the SVM and NN classifiers had an accuracy up to 100.0% for Mild_{3h} group according to their prediction confusion matrix. It demonstrated that serum-based Raman spectroscopy was a high-sensitive and effective method for the diagnosis and recognition of early mild bTBI by combined with machine learning.

Table 4 summarized the classification parameters of each classifier based on the testing set, including accuracy, sensitivity, precision. It could be seen that the diagnosis accuracy of the four classifiers were greater than 92.0%, in which the SVM classifier had the highest accuracy of 95.4%. Moreover, the sensitivities of these classifiers all were greater than 94.0%, and the highest sensitivity of SVM was up to 95.9%. Moreover, the diagnosis precisions of all classifiers were larger than 91.0%, in which the highest precision reached up to 95.7% for SVM classifier. On the whole, the classification result of SVM classifier was better than the other classifiers. As a consequence, the different degrees bTBIs at different time points can be automatically classified

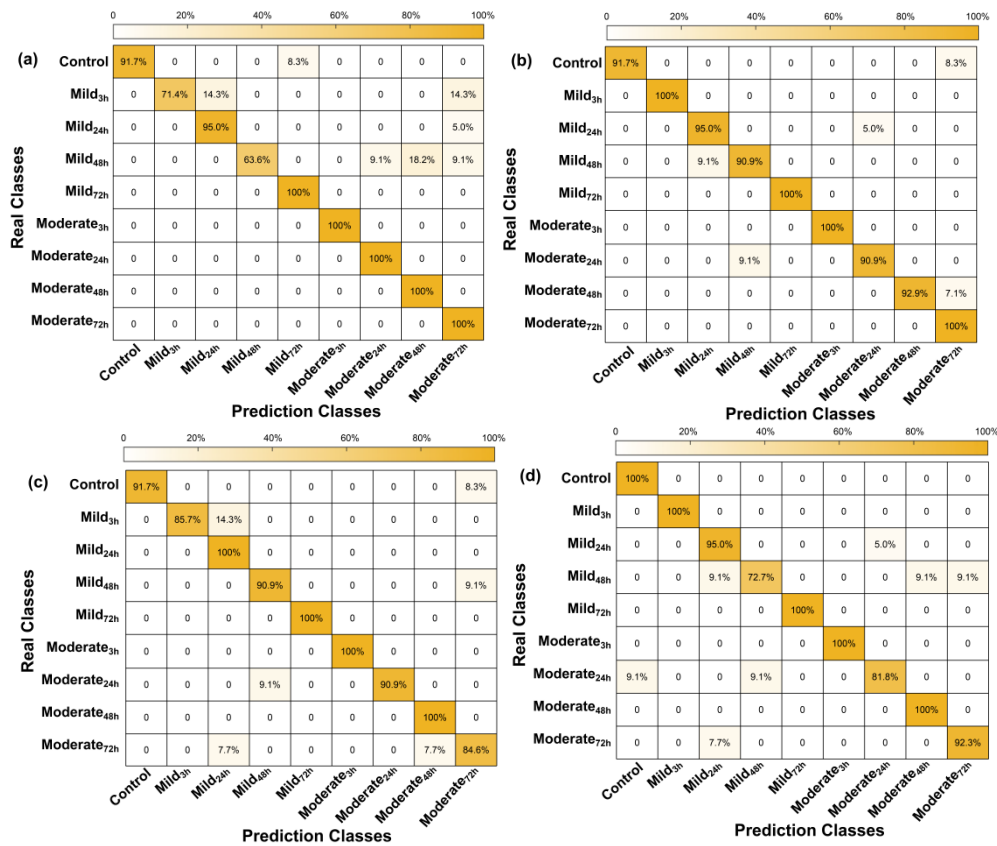


Fig. 7. The prediction confusion matrix of (a) QDA, (b) SVM, (c) *k*NN, (d) NN classifiers.

and identified based on the Raman spectra of serum samples. That is to say, the early mild bTBI can be well recognized through serum-based Raman spectroscopy. On this basis, it needs to research upon larger clinical samples in future.

Table 4. The performance parameters of each classifier based on Raman spectra of serum.

Performance parameters	Classification models			
	QDA	SVM	<i>k</i> NN	NN
Accuracy	92.7%	95.4%	94.5%	93.6%
Sensitivity	94.4%	95.9%	95.5%	94.1%
Precision	91.3%	95.7%	93.8%	93.5%

4. Conclusion

In summary, this work presented a label-free and invasion diagnosis method to recognize the different time points after different degree bTBIs based on Raman spectroscopy. The Raman spectra of serum samples in rat model were measured at 3 h, 24 h, 48 h, 72 h after mild and moderate bTBIs. The experimental results indicated that, both the position and intensity of Raman characteristic peaks exhibited apparent differences in the range of $800\text{--}3000\text{cm}^{-1}$ at 3 h, 24 h, 48 h and 72 h after mild and moderate bTBI compared with control group. This attributed

to the changes of the proteins, lipids, etc in serum after mild and moderate bTBIs. Furthermore, the QDA, SVM, *k*NN, NN classifiers after PCA were performed to automatically identify the control group, mild and moderate bTBIs at different times (a total of 9 groups). The highest accuracy, sensitivity and precision among these classifiers were up to 95.4%, 95.9% and 95.7%, respectively. Furthermore, SVM and NN classifiers had an excellent classification performance based on serum Raman spectroscopy for early mild bTBI. The results demonstrated that it was a minimal invasion method for high-sensitive and label-free automatic diagnosis of different degrees bTBI at different time points after blast exposure.

Funding. China National Funds for Distinguished Young Scientists (62175182, 62275193, U22A20123, U22A20353).

Disclosures. The authors declare no conflicts of interest.

Data availability. Data underlying the results presented in this paper are not publicly available at this time but may be obtained from the authors upon reasonable request.

Supplemental document. See [Supplement 1](#) for supporting content.

References

1. V. E. Johnson, D. F. Meaney, D. K. Cullen, and D. H. Smith, "Animal models of traumatic brain injury," *Handbook of Clinical Neurology* **127**, 115–128 (2015).
2. S. Mondello, H. Phipps, A. Wilson, T. Dittmer, and S. Hinds, "Characteristics and impact of U.S. military blast-related mild traumatic brain injury: A Systematic Review," *Front. Neurol.* **11**, 559318 (2020).
3. C. L. Mac Donald, A. M. Johnson, L. Wierzechowski, E. Kassner, T. Stewart, E. C. Nelson, N. J. Werner, O. R. Adam, D. J. Rivet, and C. S. F. Flaherty, "Outcome trends after US military concussive traumatic brain injury," *J. Neurotrauma* **34**(14), 2206–2219 (2017).
4. N. Greer, N. Sayer, E. Koeller, T. Velasquez, and T. J. Wilt, "Outcomes associated with blast versus nonblast-related traumatic brain injury in US military service members and veterans: a systematic review," *J. Head Trauma Rehab.* **33**(2), E16–E29 (2018).
5. R. J. Mullins, "Injuries from explosions: physics, biophysics, pathology, and required research focus," *J. Trauma* **66**(5), 1468–1477 (2009).
6. S. J. Tepper, "Mild traumatic brain injury in U.S. soldiers returning from Iraq: commentary," *Headache* **48**(6), 976–987 (2008).
7. L. Z. Kong, R. L. Zhang, S. H. Hu, and J. B. Lai, "Military traumatic brain injury: a challenge straddling neurology and psychiatry," *Military Med. Res.* **9**(1), 2 (2022).
8. A. Farid, P. Stefan, C. Ibolja, and D. V. Agoston, "The temporal pattern of changes in serum biomarker levels reveals complex and dynamically changing pathologies after exposure to a single low-intensity blast in mice," *Front. Neurol.* **6**, 114 (2015).
9. A. Hernandez, C. Tan, F. Plattner, A. F. Logsdon, K. Pozo, M. A. Yousuf, T. Singh, R. C. Turner, B. P. Luke-Wold, and J. D. Huber, "Exposure to mild blast forces induces neuropathological effects, neurophysiological deficits and biochemical changes," *Mol. Brain* **11**(1), 64 (2018).
10. M. M. Harper, D. Rudd, K. J. Meyer, A. G. Kanthasamy, V. Anantharam, A. A. Pieper, E. Vázquez-Rosa, M. K. Shin, K. Chaubey, and Y. Koh, "Identification of chronic brain protein changes and protein targets of serum auto-antibodies after blast-mediated traumatic brain injury," *Heliyon* **6**(2), e03374 (2020).
11. N. Balakathiresan, M. Bhomia, R. Chandran, M. Chavko, and R. K. Maheshwari, "MicroRNA Let-7i is a promising serum biomarker for blast-induced traumatic brain injury," *J. Neurotrauma* **29**(7), 1379–1387 (2012).
12. J. Weppner, M. Linsenmeyer, and W. Ide, "Military blast-related traumatic brain injury," *Curr. Phys. Med. Rehab.* **7**(4), 323–332 (2019).
13. X. Gao, J. Boryczka, P. Zheng, S. Kasani, and N. Wu, "A 'hot spot'-enhanced paper lateral flow assay for ultrasensitive detection of traumatic brain injury biomarker S-100 β in blood plasma," *Biosens. Bioelectron* **177**, 112967 (2021).
14. J. V. Rosenfeld, A. C. McFarlane, P. Bragge, R. A. Armonda, J. B. Grimes, and G. S. Ling, "Blast-related traumatic brain injury," *Lancet Neurol.* **12**(9), 882–893 (2013).
15. A. Gyorgy, G. Ling, D. Wingo, J. Walker, L. Tong, S. Parks, A. Januszkiewicz, R. Baumann, and D. V. Agoston, "Time-dependent changes in serum biomarker levels after blast traumatic brain injury," *J. Neurotrauma* **28**(6), 1121–1126 (2011).
16. W. Carr, A. M. Yarnell, R. Ong, T. Walilko, G. H. Kamimori, U. da Silva, R. M. McCarron, and M. L. LoPresti, "Ubiquitin carboxy-terminal hydrolase-L1 as a serum neurotrauma biomarker for exposure to occupational low-level blast," *Front. Neurol.* **6**, 49 (2015).
17. A. R. Stevens, C. A. Stickland, G. Harris, Z. Ahmed, P. G. Oppenheimer, A. Belli, and D. J. Davies, "Raman spectroscopy as a neuromonitoring tool in traumatic brain injury: a systematic review and clinical perspectives," *Cells* **11**(7), 1227 (2022).
18. E. Cordero, I. Latka, C. Matthaues, I. W. Schie, and J. Popp, "In-vivo Raman spectroscopy: from basics to applications," *J. Biomed. Opt.* **23**(07), 1 (2018).

19. C. Banbury, I. Styles, N. Eisenstein, E. R. Zanier, G. Vegliante, A. Belli, A. Logan, and P. G. Oppenheimer, "Spectroscopic detection of traumatic brain injury severity and biochemistry from the retina," *Biomed. Opt. Express* **11**(11), 6249–6261 (2020).
20. Y. Y. Wang, G. Q. Wang, D. Xu, T. N. Chen, and J. Q. Yao, "Terahertz spectroscopic diagnosis of early blast-induced traumatic brain injury in rat," *Biomed. Opt. Express* **11**(8), 4085–4098 (2020).
21. C. Carlomagno, D. Bertazioli, A. Gualerzi, S. Picciolini, M. Andrico, F. Roda, M. Meloni, P. I. Banfi, F. Verde, N. Ticozzi, V. Silani, E. Messina, and M. Bedoni, "Identification of the Raman salivary fingerprint of parkinson's disease through the spectroscopic-computational combinatory approach," *Front. Neurosci.* **15**, 704962 (2021).
22. Y. Qin, "A review of quadratic discriminant analysis for high-dimensional data," *WIREs Comp Stat* **10**(4), e143 (2018).
23. A. Dankowska and W. Kowalewski, "Tea types classification with data fusion of UV-Vis, synchronous fluorescence and NIR spectroscopies and chemometric analysis," *Spectrochim. Acta. A Mol. Biomol. Spectrosc.* **211**, 195–202 (2019).
24. M. A. Hearst, S. T. Dumais, E. Osuna, J. Platt, and B. Scholkopf, "Support vector machines," *IEEE Intell. Syst. Appl.* **13**(4), 18–28 (1998).
25. B. Dejaegher, L. Dhooghe, M. Goodarzi, S. Apers, L. Pieters, and Y. V. Heyden, "Classification models for neocryptolepine derivatives as inhibitors of the β -haemation formation," *Anal. Chim. Acta.* **705**(1-2), 98–110 (2011).
26. S. Karamizadeh, S. M. Abdullah, M. Halimi, J. Shayan, and M. J. Rajabi, "Advantage and drawback of support vector machine functionality," *Proc. IEEE*, 63–65 (2014).
27. M. L. Zhang and Z. H. Zhou, "ML-KNN: A lazy learning approach to multi-label learning," *Pattern Recognit.* **40**(7), 2038–2048 (2007).
28. G. Cho, J. Yim, Y. Y. Choi, J. Ko, and S. H. Lee, "Review of machine learning algorithms for diagnosing mental illness," *Psychiatry Investig.* **16**(4), 262–269 (2019).
29. S. A. Mojarad, S. S. Dlay, W. L. Woo, and G. V. Sherbet, "Cross validation evaluation for breast cancer prediction using multilayer perceptron neural networks," *Am. J. Engg. & Applied Sci.* **4**(4), 576–585 (2011).
30. L. N. Li, X. F. Liu, F. Yang, W. M. Xu, J. Y. Wang, and R. Shu, "A review of artificial neural network based chemometrics applied in laser-induced breakdown spectroscopy analysis," *Spectrochim. Acta, Part B* **180**, 106183 (2021).
31. Y. Zhao and K. Wang, "Fast cross validation for regularized extreme learning machine," *J. Syst. Eng. Electron.* **25**(5), 895–900 (2014).
32. L. F. Santos, R. Wolthuis, S. Koljenovic, R. M. Almeida, and G. J. Puppels, "Fiber-optic probes for in vivo Raman spectroscopy in the high-wavenumber region," *Anal. Chem.* **77**(20), 6747–6752 (2005).
33. J. M. Surmacki, L. Ansel-Bollepalli, F. Pischiutta, E. R. Zanier, A. Ercole, and S. E. Bohndiek, "Label-free monitoring of tissue biochemistry following traumatic brain injury using Raman spectroscopy," *Analyst* **142**(1), 132–139 (2017).
34. A. Chaichi, S. M. A. Hasan, N. Mehta, F. Donnarumma, P. Ebenezer, K. K. Murray, J. Francis, and M. R. Gartia, "Label-free lipidome study of paraventricular thalamic nucleus (PVT) of rat brain with post-traumatic stress injury by Raman imaging," *Analyst* **146**(1), 170–183 (2021).
35. O. Uckermann, W. Yao, T. A. Juratli, R. Galli, E. Leipnitz, M. Meinhardt, E. Koch, G. Schackert, G. Steiner, and M. Kirsch, "IDH1 mutation in human glioma induces chemical alterations that are amenable to optical Raman spectroscopy," *J. Neuro-Oncol.* **139**(2), 261–268 (2018).
36. S. N. Kalkanis, R. E. Kast, M. L. Rosenblum, T. Mikkelsen, S. M. Yurgelevic, K. M. Nelson, A. Raghunathan, L. M. Poisson, and G. W. Auner, "Raman spectroscopy to distinguish grey matter, necrosis, and glioblastoma multiforme in frozen tissue sections," *J. Neuro-Oncol.* **116**(3), 477–485 (2014).
37. Y. Zhou, C. Liu, B. Wu, X. Yu, G. Cheng, K. Zhu, K. Wang, C. Zhang, M. Zhao, R. Zong, L. Zhang, L. Shi, and Robert R. Alfano, "Optical biopsy identification and grading of gliomas using label-free visible resonance Raman spectroscopy," *J. Biomed. Opt.* **24**(09), 1 (2019).